



ELSEVIER

Contents lists available at ScienceDirect

Journal of Quantitative Spectroscopy & Radiative Transfer

journal homepage: www.elsevier.com/locate/jqsrt

Comparisons of PBL heights derived from CALIPSO and ECMWF reanalysis data over China

Jingjing Liu, Jianping Huang*, Bin Chen, Tian Zhou, Hongru Yan, Hongchun Jin, Zhongwei Huang, Beidou Zhang

Key Laboratory for Semi-Arid Climate Change of the Ministry of Education, College of Atmospheric Sciences, Lanzhou University, Lanzhou 730000, China

ARTICLE INFO

Article history:

Received 14 May 2014
Received in revised form
27 September 2014
Accepted 13 October 2014
Available online 27 October 2014

Keywords:

CALIPSO
PBL
ECMWF

ABSTRACT

Planetary boundary layer (PBL) height was estimated using the maximum standard deviation method for Cloud–Aerosol Lidar and Infrared Pathfinder Satellite Observation (CALIPSO) attenuated backscatter observations. It was only retrieved under conditions where the clouds accounted for less than 5% in a profile, where it could be compared with ground lidar results at SACOL. The correlation between CALIPSO and the ground lidar was 0.73. We present the seasonal mean patterns of 4-year mid-day PBL heights over China and use them to evaluate the European Centre for Medium-Range Weather Forecasts (ECMWF) PBL depth retrievals, inform boundary layer studies, and improve our understanding of how PBL height mediates exchanges of energy and pollutants between the surface and the atmosphere. We found that the largest PBL heights occurred over the Tibetan Plateau and coastal areas. The smallest PBL heights appeared in the Tarim Basin and northeast of China during local winter. A comparison of CALIPSO and ECMWF PBL under different land-cover conditions showed that the PBL depth estimated by the CALIPSO backscatter climatology is larger over ocean and forest surface than that estimated from ECMWF data. However, the PBL heights of ECMWF that were larger than those of CALIPSO were mainly concentrated over grassland and bare land surface in spring and summer.

© 2014 Elsevier Ltd. All rights reserved.

1. Introduction

The PBL is an important parameter in the Earth's climate system, mediating exchanges of energy, moisture, momentum, carbon, and pollutants between the surface and the overlying atmosphere. The PBL acts as a barrier to surface-emitted pollutants, leading to high concentrations within the PBL [40]. In addition, cloud processes, land and ocean surface fluxes and the atmospheric hydrological cycle in general are strongly influenced by the boundary layer. Hence, estimates of

the PBL play a role in weather and air quality forecasts. However, one major issue in this context is the lack of global observational datasets. Measuring the PBL top in situ is not a trivial endeavor. Therefore, the atmospheric boundary layer has been notoriously difficult to observe from space [39,22,32], preventing a detailed understanding of its properties on global scales. Considering the sensitivity and importance of the PBL depth to specific spatial and temporal conditions, it must be taken into account when verifying PBL outputs from models. It also complicates the evaluations of observing systems. Meanwhile, observation of the PBL height serves as a diagnostic tool with respect to the physics and dynamics packages in a model. However, model developers are uncertain of the precision of model PBL height

* Correspondence to: College of Atmospheric Sciences, Lanzhou University, Lanzhou 730000, China. Tel.: +86 931 891 4282.
E-mail address: hjp@lzu.edu.cn (J. Huang).

predictions because verification by direct observations of the PBL height is difficult.

Space-borne lidar is sensitive to atmosphere aerosols and boundary layer clouds that can be used to identify the PBL top. It has been used to provide information on the depth of the layer, and it is a valuable tool for observing PBL depths on multiple platforms [2]. A few limited-scale studies have examined PBL processes using space-based remote sensing [30]. Estimates of the PBL height for two regions of the subtropical and tropical eastern Pacific were presented using satellite observations from the Moderate Resolution Imaging Spectroradiometer (MODIS) and the Tropical Rainfall Measuring Mission (TRMM) Microwave Imager (TMI) [52]. Jordan et al. [22] validated PBL depth derived from CALIPSO measurements by ground-based lidar and radiosonde data at the University of Maryland, Baltimore County, and reported daytime PBL heights over the Western Hemisphere and Africa, the first large-scale observational study of PBL heights using CALIPSO measurements. Afterwards, McGrath-Spangler and Denning [32] determined PBL depths over North America during summertime using a modified method from Jordan et al. [22] by CALIPSO measurements. McGrath-Spangler, Denning [33] extended the method to produce a global analysis of PBL depths and consider regional variations throughout the year. Guo et al. [8] used radio occultation data from Global Positioning System (GPS) satellites to determine the PBL depth over the ocean. These retrievals compared favorably with radiosonde data, producing a correlation coefficient of about 0.82. Chan and Wood [4] applied an algorithm to determine the global seasonal cycle of PBL depth by the maximum vertical gradient of refractivity from Constellation Observing System for Meteorology, the Ionosphere, and Climate (COSMIC) satellite mission measurements.

Some studies of boundary layer properties from space-based remote sensing instruments have also been used to validate PBL estimates by models. Randall et al. [38] compared the boundary layer height derived from the LITE data with output from the Colorado State University atmospheric general circulation model, as well as the National Center for Atmospheric Research (NCAR) Community Climate Model 3 (CCM3). Palm et al. [37] showed that the Geoscience Laser Altimeter System (GLAS)-derived boundary layer height over the oceans is generally 200–400 m higher than the model predictions, but small-scale and global patterns of PBL height show similar features. Jordan et al. [22] compared CALIPSO PBL heights to matched PBL heights from the Goddard Earth Observing System-version 5 (GEOS-5) Modern Era Reanalysis for Research and Applications (MERRA) model in the Western Hemisphere and over Africa. They revealed that GEOS-5 predicts PBL heights within 25% of CALIPSO observations for much of the study region and GEOS-5/CALIPSO PBL height ratios exceed 1.25 in the equatorial Pacific. Ao et al. [2] also performed an analysis using GPS data to produce a global climatology of PBL heights and compared them with values calculated from the ECMWF Reanalysis Interim (ERA-Int). Leventidou et al. [26] compared PBL heights retrieved from CALIPSO, ECMWF, and radiosondes over Thessaloniki, Greece.

Overall, little large-scale research about the PBL height over China has been performed. The complex topography in China is a challenge for correct derivation of PBL depths for routine observations. The CALIPSO observations have the potential to expand our knowledge about PBL processes by providing a global dataset. Here, we extend and modify the maximum standard deviation method of Jordan et al. [22] to estimate PBL heights over China (20–50°N, 75–135°E) from CALIPSO measurements. The following section provides a brief description of the method used to derive the PBL depth from the CALIPSO satellite and the National Institute for Environmental Studies (NIES) lidar, a ground-based lidar located at the Semi-Arid Climate and Environment Observatory of Lanzhou University (SACOL). Section 3 presents the results of comparisons of the CALIPSO, NIES lidar and ECMWF PBL. Conclusions are provided in the final section.

2. Data and methods

2.1. PBL heights from ECMWF

ECMWF Interim Re-Analysis (ERA-Interim) systems assimilate a variety of information into weather prediction models, ranging from in situ to space-based instruments. These provide a global climatology for PBL height and are important for the physics of the boundary layer from a global perspective and evaluation of weather and climate prediction models.

ECMWF models define the top of the PBL as the level where the bulk-Richardson number, based on the difference between quantities at that level and the lowest model level, reaches a critical value of 0.25 [46]. The bulk Richardson number is essentially the ratio of stability to vertical wind shear. It may reach this critical value at a height somewhat below the PBL top as defined by other means [37]. If the BL height is found to be between two model values, the exact height is calculated through linear interpolation.

The precision of model PBL height predictions is poor because verification by direct observations of the PBL height is rare. Here, CALIPSO PBL are directly used to perform further validations and comparisons with the PBL height variable from ECMWF ERA-Interim fields for the years 2007–2010 in this study. ECMWF provides PBL heights at 6-hourly intervals (0:00 UTC, 6:00 UTC etc.) with $0.75^\circ \times 0.75^\circ$ latitude–longitude resolution. Because the Coordinated Universal Time (UTC) at which CALIPSO passes by the SACOL [17,21,9] is approximately 6:25 UTC, with a local solar time (LST) of 14:25, PBL heights at 6:00 UTC from ECMWF were used in this study.

2.2. PBL heights from CALIPSO

CALIPSO is part of NASA's Afternoon constellation (A-Train) of satellites. It is in a 705-km sun-synchronous polar orbit with an equator crossing time of about 1:30 P.M. LST and a 16-day repeat cycle [50,51,20]. The CALIPSO satellite has three instruments: a cloud–aerosol lidar with orthogonal polarization (CALIOP), an Imaging Infrared Radiometer (IIR), and a moderate spatial resolution wide

field camera (WFC). CALIOP's ability to accurately retrieve vertical distributions of aerosols and clouds at high vertical resolution makes it a superb platform for reducing uncertainty in the climate system [49,16,18,19,28]. The CALIOP lidar backscatter data were recorded at 532 nm (parallel and perpendicular polarization) and at 1064 nm, which and were used to derive information about the depolarization ratio [11,43] and color ratio of particles, creating a useful requirement for evaluation of the maximum PBL depth. The products used in this analysis were the Version 3.01 4-year (2007–2010) Level 1B data and Level 2 vertical feature mask (VFM) daytime observations data. VFM data contain vertical distributions of clouds and aerosols; studies have confirmed that clouds and aerosols can be discriminated correctly in VFM data [5,6,27]. Daytime observations were used from CALIPSO to ensure that residual layers were not picked out in nighttime data. Residual layers at night were most closely related to daytime maximum PBL heights. The matchup of the position of the PBL in daytime with a nighttime retrieval would needlessly complicate this analysis by requiring the computation of transport over a 12-h period from a prior day PBL maximum [22].

In general, the PBL is capped by a temperature inversion that tends to trap moisture and aerosols [7]. The gradient of backscatter seen by lidar is almost always associated with this temperature inversion and the simultaneous decrease in moisture content [36,34]. Thus, the definition of the PBL top as the location of the maximum aerosol scattering gradient is analogous to the more conventional thermodynamic definition. Jordan et al. [22] first developed a method for deriving the PBL by a maximum standard deviation technique using CALIPSO 532-nm attenuated backscatter. This was based on an idea by Melfi et al. [34] that at the top of the PBL, there is a maximum in the vertical standard deviation of lidar backscatter. This method was compared with the GEOS-5 Modern

Era Reanalysis for Research and Applications (MERRA) model. Extensive comparisons between the model output and satellite observations in the Western Hemisphere and over Africa gave model–measurement correlation coefficients (R) of 0.47–0.73. However, Jordan evaluated their CALIPSO-based PBL retrieval by visual inspection. McGrath-Spangler and Denning [32] automated the algorithm to process a larger subset of the available data.

We used the above method to calculate the PBL heights in China using CALIPSO data. The detailed process is seen in Fig. 1. First, we acquired 532-nm attenuated backscatter and VFM data by CALIPSO lidar measurements. Then, we added a check to eliminate surface noise; the signal-to-noise ratio (SNR) in the backscatter is low close to the Earth's surface [23]. We adopted surface elevation data from 532-nm attenuated backscatter to eliminate the apparent signal return below the surface due to imperfect electronics [31]. Meanwhile, we selected profiles with a clear aerosol signature within a reasonable height range, and removed clouds containing large signal attenuation [10,13–15] by VFM data. In contrast, McGrath-Spangler and Denning [32] defined optically thick clouds by the occurrence of three vertically consecutive layers with a 1064-nm backscatter value exceeding $10^{-2.25} \text{ km}^{-1} \text{ sr}^{-1}$. The 1064-nm data were used by Okamoto et al. [35] to identify cloud layers based on a mid-latitude case study during the MRO1/KO2 cruise of the research vessel Mirai. Therefore, considering the result with regional characteristics from Okamoto et al. [35], we made a modification such that clouds with large signal attenuation were removed by Level 2 VFM data [11,12], the detailed process for which is seen in Fig. 2.

Fig. 2 shows a case study of our PBL depth estimation process for a March 4, 2007 overpass of the satellite across China. The dark blue regions near the bottom of the figure

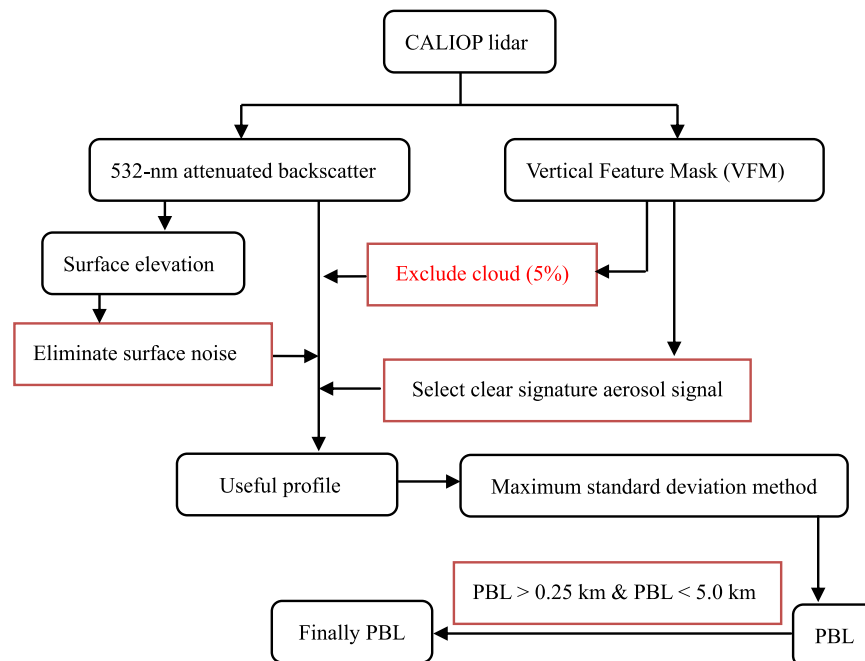


Fig. 1. Flow chart of derive PBL height from CALIPSO data.

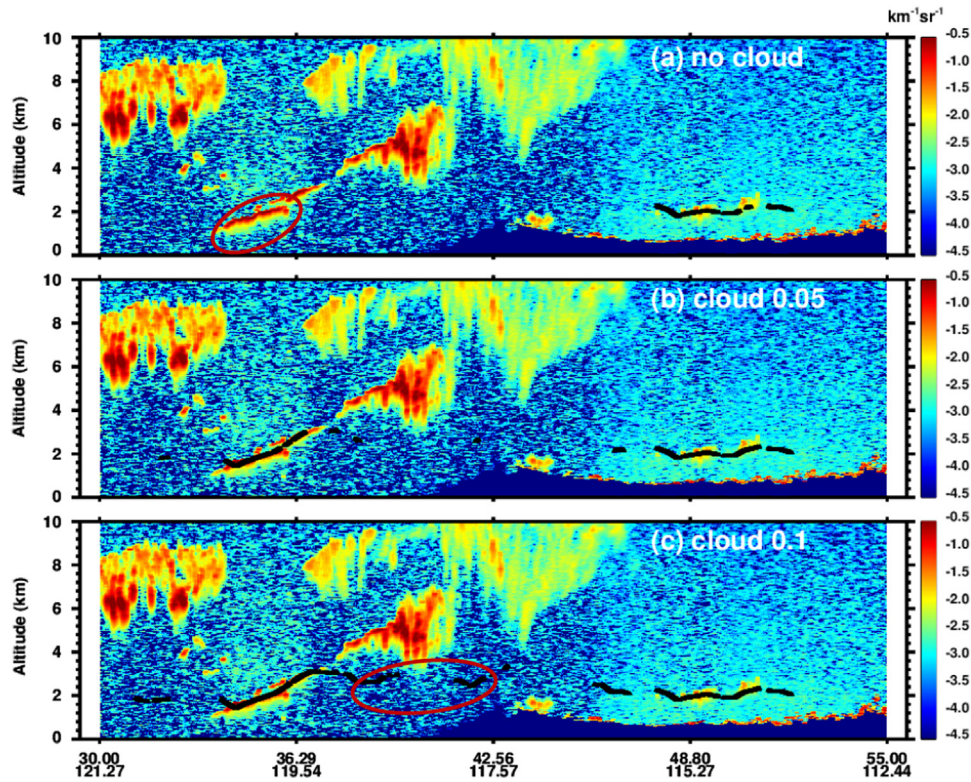


Fig. 2. CALIPSO PBL height derived by combining level 1 532-nm attenuated backscatter and level 2 vertical feature mask (VFM) using the maximum variance method in March 4, 2007. (For interpretation of the references to color in this figure, the reader is referred to the web version of this article.)

indicate the surface elevation available in the level 1B product. There was a strong backscatter signal at the level where the lidar beam reached the solid surface, which was removed by surface elevation data. Then, we eliminated profiles with large signal attenuation due to clouds and without a clear aerosol signature within a reasonable height range by VFM data. Then, three different threshold values, which were calculated using total cloud numbers in a vertical profile divided by total bins, 0% [Fig. 2(a)], < 5% [Fig. 2(b)], and 10% [Fig. 2(c)], were chosen, with the aim of achieving a more reasonable value for eliminating the clouds and calculating the PBL depth. The black line indicates the PBL depth estimated by the algorithm with each threshold. No PBL values are shown if no valid value was retrieved. In Fig. 2(a), some credible signal-to-noise ratio regions, represented by the red circle, were ignored. However, some regions with low signal-to-noise ratios (red circle), where some optically thick feature layers attenuated the lidar signal, were used to calculate the PBL depth, leading to lower confidence in Fig. 2(c). In summary, 5% is the most reasonable threshold for calculating the PBL depth. It accurately locates the backscatter signal indicating the PBL top. This result is also supported by Yan et al. [53], who indicated that clear-sky conditions are defined as having a cloud fraction < 5%, whereas cloudy conditions have cloud fractions > 5%. Finally, those PBL heights > 5 km or < 0.25 km were instead assigned a missing value, as in McGrath-Spangler and Denning [32].

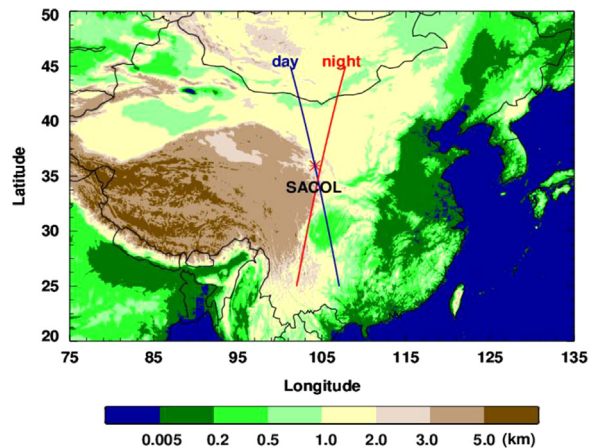


Fig. 3. The location of SACOL lidar (the red asterisk) and tracks of CALIPSO (blue color: daytime, red color: nighttime). (For interpretation of the references to color in this figure legend, the reader is referred to the web version of this article.)

2.3. PBL heights from NIES lidar

To evaluate the contributions from unknown desert sources and assess transportation routes, many lidar stations have recently been constructed, and collaborative measurements have been performed. Since 2001, the National Institute for Environmental Studies (NIES) in

Japan has been expanding the Asian Dust and aerosol lidar observation Network (AD-Net) [41,44,24]. At present, more than 20 lidar stations in Japan, Korea, and China are in the network [42]. The NIES lidar at the SACOL is a two-wavelength (532 nm and 1064 nm) Mie-scattering lidar with polarization channels at 532 nm that has been applied since June 2009. This lidar system mainly consists of a high-powered Nd:Yag laser, a 200-mm telescope, and an optical spectrometer with vertical and parallel depolarization channels at two wavelengths, consistent with CALIPSO. Therefore, a 532-nm and 1064-nm attenuated backscatter coefficient, depolarization ratio, and color ratio can be derived by NIES lidar. Fig. 3 shows the topography of SACOL and the CALIPSO orbits (blue color represents daytime, and red color represents nighttime) near the NIES lidar sites. The ground-based NIES lidar at SACOL is located at 35.57°N, 104.08°W, and the surface elevation is 1966 m. The CALIPSO overpass time near SACOL is about 6:25 UTC. The nearest distance from the CALIPSO ground track to the lidar site is ~ 3 km during the day, on average. The NIES lidar PBL height is calculated from the elastic scattering returns in a 532-nm channel, with the largest standard deviation method used to retrieve the CALIPSO PBL heights. However, problems with surface elevation and optically thick clouds are unimportant for upward-looking

NIES lidar. Data from NIES lidar measurements throughout 2010 are used to compare with the CALIPSO PBL in this study.

3. Results

We compared PBL heights from 17-day coincident NIES lidar observations with data from CALIOP/CALIPSO passing by the SACOL in 2010 and validated the ECWMF PBL heights. Meanwhile, we also compared the seasonal PBL height distribution from the ECMWF reanalysis data with the PBL height determined from CALIPSO measurements in China from 2007 to 2010.

Fig. 4 shows a case study of the NIES ground-based lidar profile, which contains the attenuated backscatter coefficient (a), the depolarization ratio (b), and the color ratio (c) distributions observed from NIES lidar, with the PBL height (black dotted line) derived via the maximum standard deviation method on November 13, 2010. Clear aerosol signature layers located at 1–2 km and cloud layers around 6–10 km are shown. The NIES lidar PBL heights generally match with the aerosol vertical structures. The vertical white line corresponds to the closest point of approach of CALIPSO to the NIES lidar at 6:24 UTC. Because the NIES lidar sample time resolution is 15 min, the 6:30

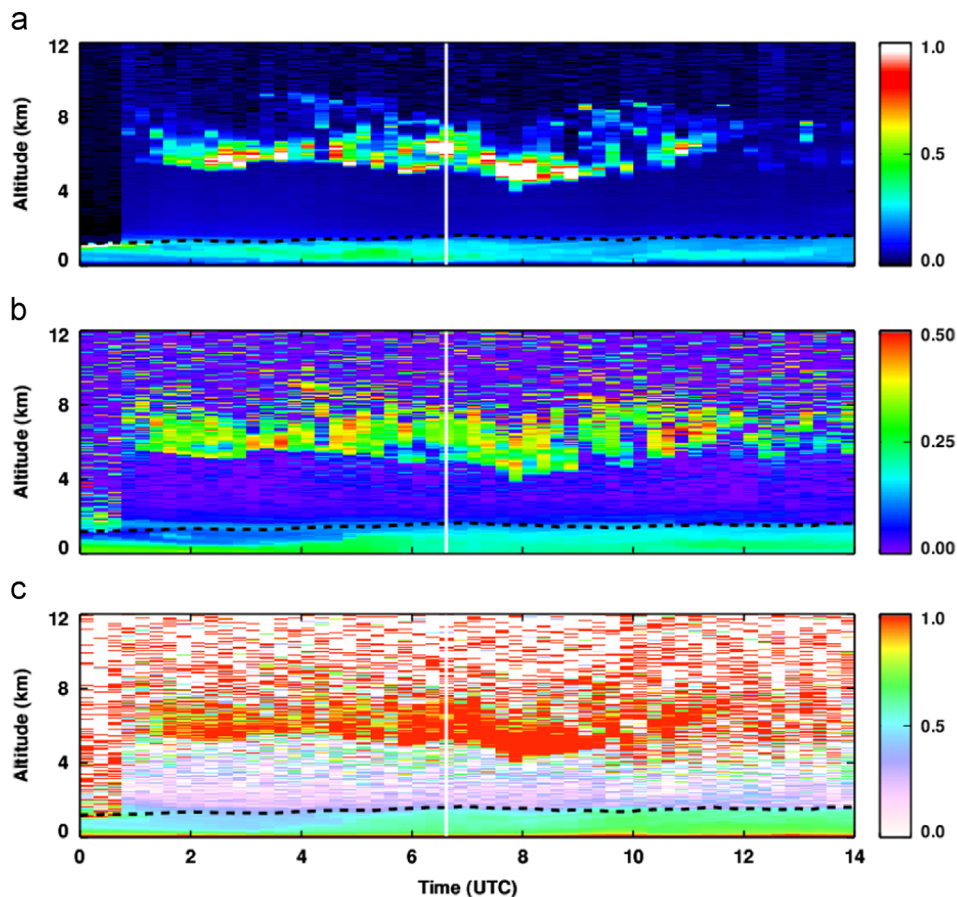


Fig. 4. (a) Attenuated backscatter coefficient, (b) depolarization ratio, @ 532nm and (c) color ratio (1064nm/532nm) observed from NIES ground-base lidar in Nov. 13, 2010. The black dotted line indicates NIES lidar PBL height via maximum standard deviation method, and the white vertical line corresponds to the closest point of CALIPSO to NIES lidar at SACOL. (For interpretation of the references to color in this figure legend, the reader is referred to the web version of this article.)

UTC profile from NIES lidar was chosen. At that time, the NIES PBL height determined by the standard deviation method was ~ 1.2 km, and the CALIPSO PBL height was 1.1 km. This result revealed that the ground-based PBL was in close agreement with the CALIPSO lidar, consistent with Jordan et al. [22].

To validate ECMWF reanalysis data, the PBL height values retrieved from CALIPSO and from ECMWF were compared with those derived from NIES lidar. We obtained 17-day ground-based lidar observations coincident with the CALIOP/CALIPSO passing by the NIES lidar in 2010. The majority of data account for PBL heights lower than 3.0 km. Fig. 5 shows a day-by-day comparison and correlation of the CALIPSO, NIES-ground lidar PBL, and ECMWF PBL reanalysis data in the daytime. Close agreement is indicated between CALIPSO and NIES lidar, with a correlation coefficient of 0.73 in Fig. 5(b). The scatter plot shows a lower correlation between ECMWF and NIES than does Fig. 5(b), with a correlation coefficient (R) of 0.57 in Fig. 5(d). Meanwhile, correlation coefficient between CALIPSO and ECMWF is 0.58, presented in Fig. 5(c).

The PBL depth can change by a kilometer or more in as little as 1 h [48], and a point measurement may not be representative of the spatial average [1,48]. It is therefore imperative to validate the PBL height spatial distributions of the model with other observational data (e.g. satellite) that are as close to coincident as possible. Next, we estimate the PBL height seasonal distributions in China from 2007 to 2010 and compare them with the ECMWF PBL heights.

Spatial patterns of 4-year (2007–2010) mean mid-day PBL heights over China were estimated by combining the CALIPSO lidar backscatter and VFM data presented in Fig. 6. PBL heights associated with aerosol and shallow clouds during mid-day CALIPSO overpasses were estimated and were only retrieved in the absence of optically thick cloud. This result is an average of the instantaneous values to show the general behavior, but the individual values themselves provide a climatology distribution ($1.5^\circ \times 1.5^\circ$) for the PBL depth. These estimates are relative to the surface height. We found that higher PBL height values occur over land rather than over water. This result is

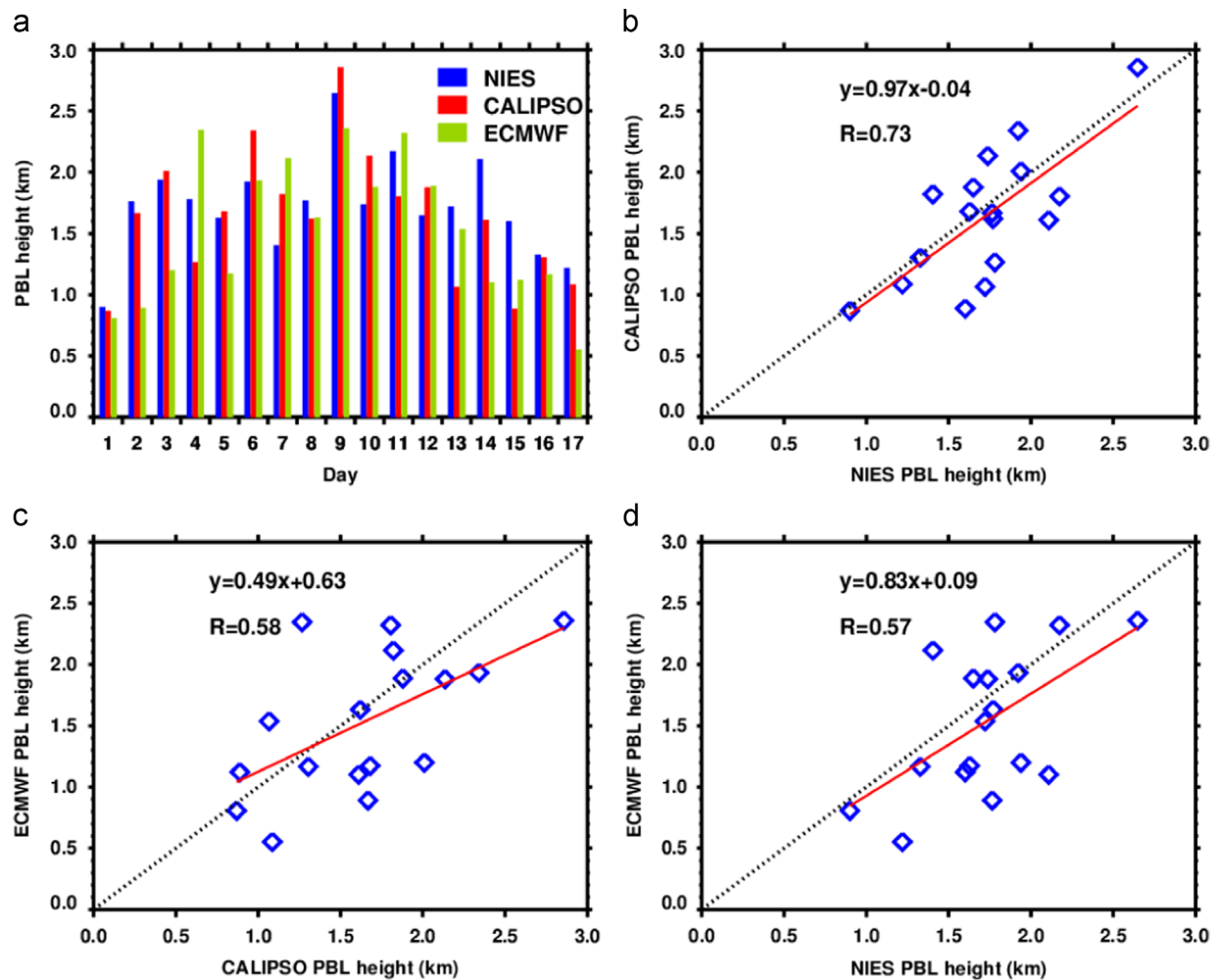


Fig. 5. (a) Comparison and correlation of the NIES PBL, CALIPSO-derived PBL and ECMWF PBL in the day near the SACOL site in 2010.

planetary boundary depth from CALIPSO during 2007-2010

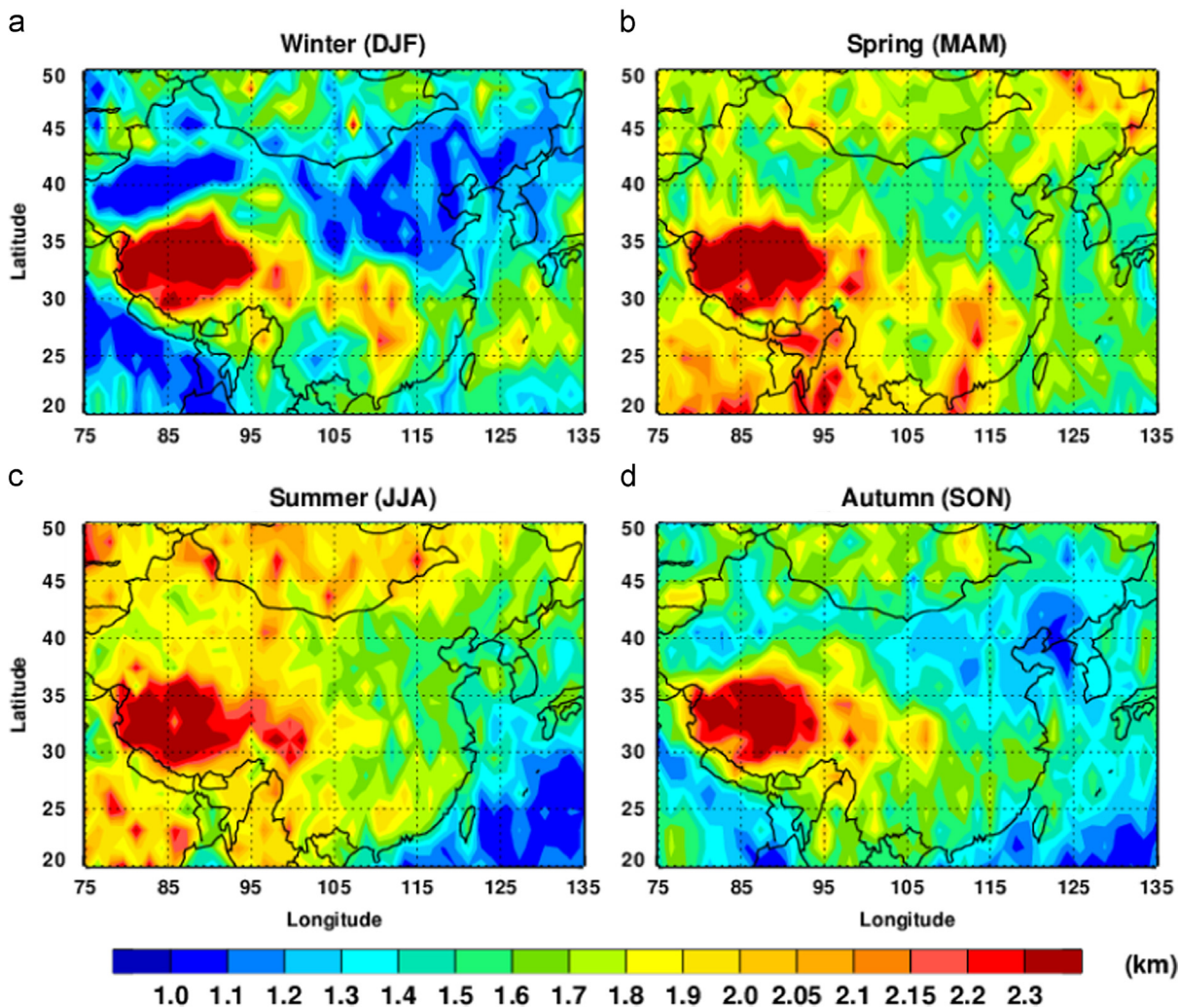


Fig. 6. Spatial patterns of 4-year (2007–2010) seasonal mean mid-day PBL depths ($1.5^\circ \times 1.5^\circ$) over China were estimated from the CALIPSO.

consistent with [32]. The deepest PBL depths occur over the Tibetan Plateau are seen from the whole-year distribution, and coastal areas in spring and winter. A possible explanation is that the Tibet Plateau acts as a local heat source, and urbanization of coastal areas contributes to the development of the PBL height. In general, seasonal variance in the PBL height is significant. The PBL heights in summer are greatest, revealing that incoming solar radiation is a major factor in producing more available energy for strong turbulence. Higher values of the PBL height are reached in summer over dry subtropical land regions (larger than 2.1 km). Some studies also revealed that the higher Bowen ratio and amount of solar radiation create a situation in which deeper than expected (over 2 km) PBL depths occur in June during the Boreal Ecosystem-Atmosphere Study (BOREAS) field experiment [e.g., [3,29]]. The Bowen ratio is used to describe the type of heat transfer and is defined as the ratio of sensible heat flux to latent heat flux. The lowest mean values of the PBL

height appeared in the Tarim Basin and Northeast of China during local winter. Over the oceans, PBL heights show an opposite seasonal cycle with land (greatest in winter and lowest in summer). The PBL height in winter is presumably associated with baroclinic systems [47]. During the northern hemisphere summer, oceans are dominated by fog [25,45] and as such have fairly low PBL heights values.

Fig. 7 shows a histogram of the PBL depths from CALIPSO (a) and ECMWF (b). For CALIPSO, the probability distribution frequency (PDF) reaches a maximum at 1.25–1.5 km. For ECMWF, the PBL depths are biased toward shallower depths, with a maximum at 0.75–1.0 km. This illustrates that the CALIPSO PBL height is larger than that of the ECWmf as a whole.

Fig. 8 shows the ratio of ECMWF reanalysis PBL depths to the PBL-associated backscatter heights derived from CALIPSO. The reanalysis product estimates are significantly lower than those from CALIPSO lidar-based PBL depth over the oceans and coastal areas. In spring and summer, PBL

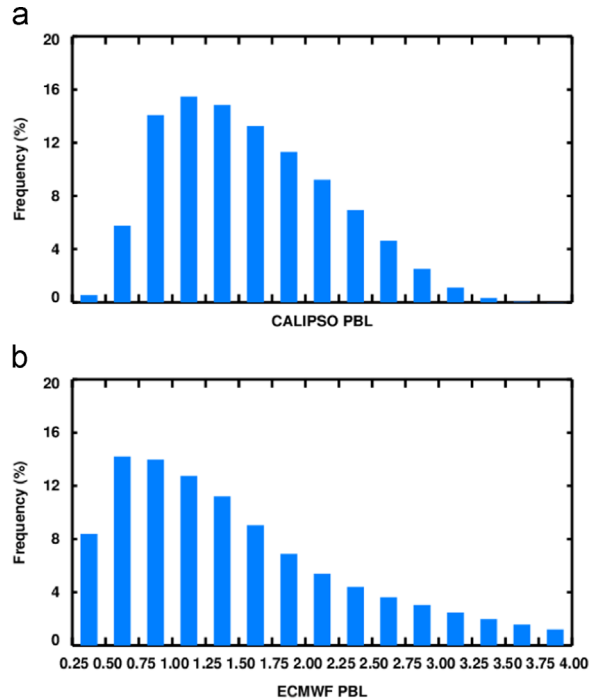


Fig. 7. Histogram plots that show (a) the CALIPSO and (b) ECMWF annual mean PBL percentage frequency for the China from 2007 to 2010.

heights from ECMWF are larger than those from CALIPSO over North China. During autumn, a majority of the ECMWF PBL depths are within 25% of the estimates derived from CALIPSO. Next, we will analyze which land cover has the largest influence on differences in the seasonal variation between ECMWF and CALIPSO PBL heights.

The vegetation types in China as determined by MODIS at 0.05° spatial resolution are plotted in Fig. 9, including 18 different surface types (0: water; 1: evergreen needleleaf; 2: evergreen broadleaf; 3: deciduous needleleaf; 4: deciduous broadleaf; 5: mixed forest; 6: closed shrublands; 7: open shrublands; 8: woody savannas; 9: savannas; 10: grasslands; 11: permanent wetlands; 12: croplands; 13: urban and built-up; 14: cropland mosaics; 15: snow and ice; 16: bare sparsely vegetated; 17: unclassified). We integrated these land covers forms into five main types: water (0), forest (1–7), grassland (8–10), cropland (12, 14), and bare vegetation (16). Seasonal differences between CALIPSO and ECMWF PBL under the condition of different land covers are presented in Fig. 10, and detailed values are listed in Table 1. We found that the largest differences occurred over bare land surfaces in summer, with the largest overestimate (0.97), and over water surface in spring, with the greatest underestimate (-0.91) compared with CALIPSO. In general, the PBL heights of ECMWF that were larger than those of CALIPSO were mainly concentrated over grassland and bare land surfaces in spring and summer. Negative values for ECMWF PBL minus CALIPSO PBL were found for nearly all land covers in autumn and winter, and for water and forest all year round. Overall, the

best correlation occurred over cropland, and the worst over water surface.

4. Conclusions and discussions

In this paper, we derived PBL heights in the China region from CALIPSO by the modified maximum standard deviation method. The PBL height values retrieved from CALIPSO that were coincident with SACOL and ECMWF observations were compared with those derived from NIES lidar. An observational study of PBL heights using CALIPSO with comparisons to ECMWF reanalysis data over China was also presented. Thus, the present research provides better insight into the PBL height variance in the ECMWF reanalysis data.

We obtained 17-day coincident ground-based lidar observations with CALIOP/CALIPSO passing by the NIES in 2010. Correlation between the CALIPSO and NIES-ground lidar PBL in the daytime reached 0.73. ECMWF and NIES correlations were lower (0.57, on average).

The PBL height distributions in China from CALIPSO showed significant seasonal variance. The deepest PBL depths occurred over the Tibet Plateau and coastal areas. PBL heights in summer were the greatest, indicating that incoming solar radiation is a major factor in producing more available energy for strong turbulence [3,29]. The lowest mean values of PBL height appeared in the Tarim Basin and Northeast of China during local winter. Over the oceans, PBL heights had the opposite seasonal cycle (largest in winter and lowest in summer). The PBL height in winter is presumably associated with baroclinic systems [47], and oceans are dominated by fog in summer [25,45].

Climate modelers are constantly searching for new opportunities to verify model outputs. Therefore, CALIPSO PBL heights and ECMWF reanalysis data were compared. A significant disagreement between ECMWF PBL height and CALIPSO was noted over coastal areas and over North China. Comparing CALIPSO and ECMWF PBL seasonal distributions under different land-cover conditions, we also found that the PBL depth estimate by the CALIPSO backscatter climatology over water and forest surface was greater than that from ECMWF. The best correlation occurred over cropland, and the worst correlation occurred over water surface, which showed a significant overestimate.

This algorithm has several weaknesses that should be considered when applying these results (seen in McGrath-Spangler and Denning [32]). The PBL depth can change by a kilometer or more in as little as 1 h [48], and a point measurement may not be representative of the spatial average [1,48]. This sensitivity of the PBL depth to specific spatial and temporal conditions must be taken into account when doing comparisons, and it complicates evaluations of the observing systems. It is therefore imperative to validate the spatial distribution of modeled PBL heights by other observations data (e.g., satellite) that are as nearly coincident as possible. Because it is nearly impossible to obtain observations that coincide perfectly in both space and time, this complexity should be kept in mind. Despite these limitations, initial estimates of a PBL depth using the methodology of Jordan et al. [22] seem

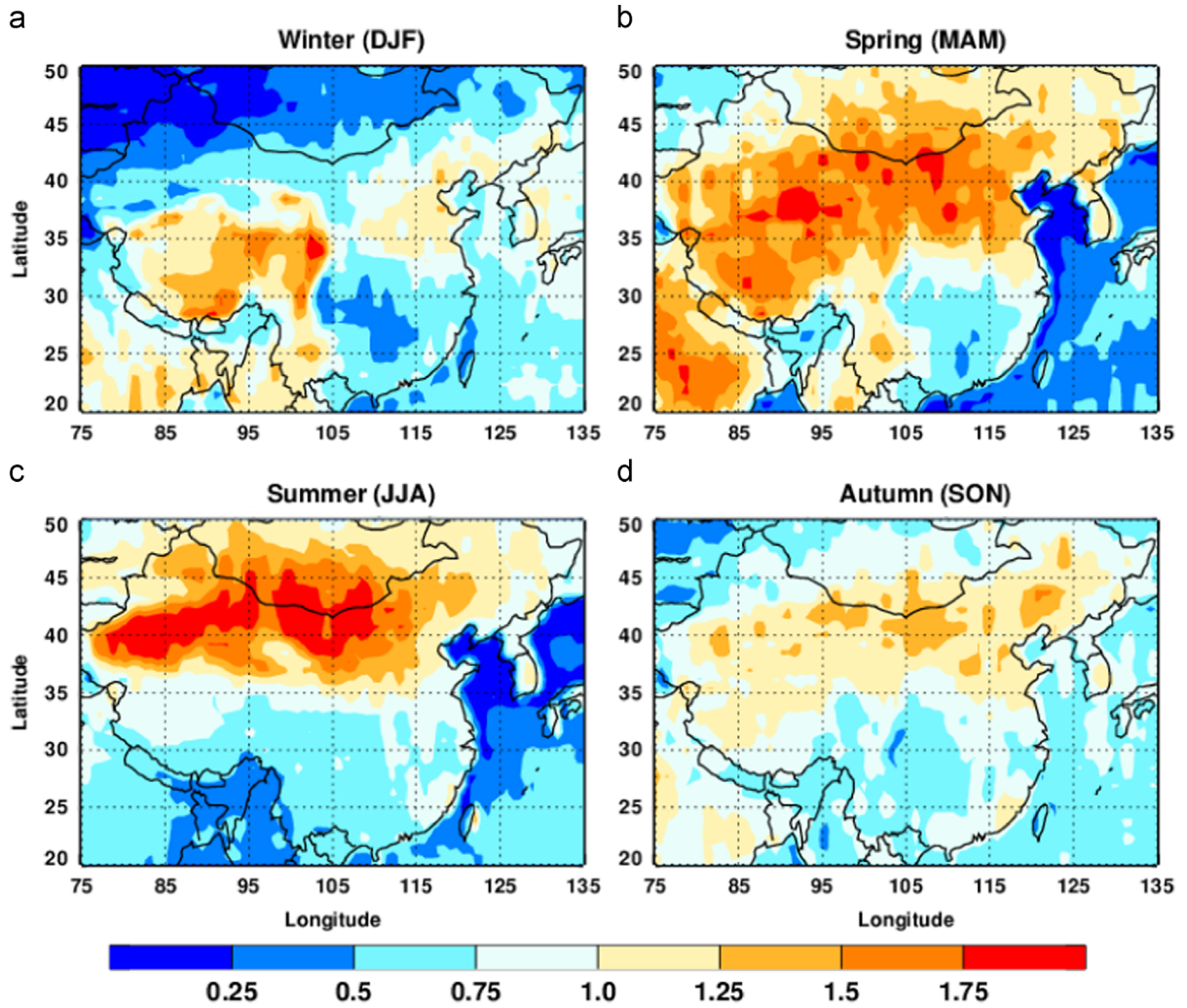


Fig. 8. The seasonal ratio of ECMWF reanalysis PBL depths to CALIPSO estimates of PBL depth from 2007 to 2010.

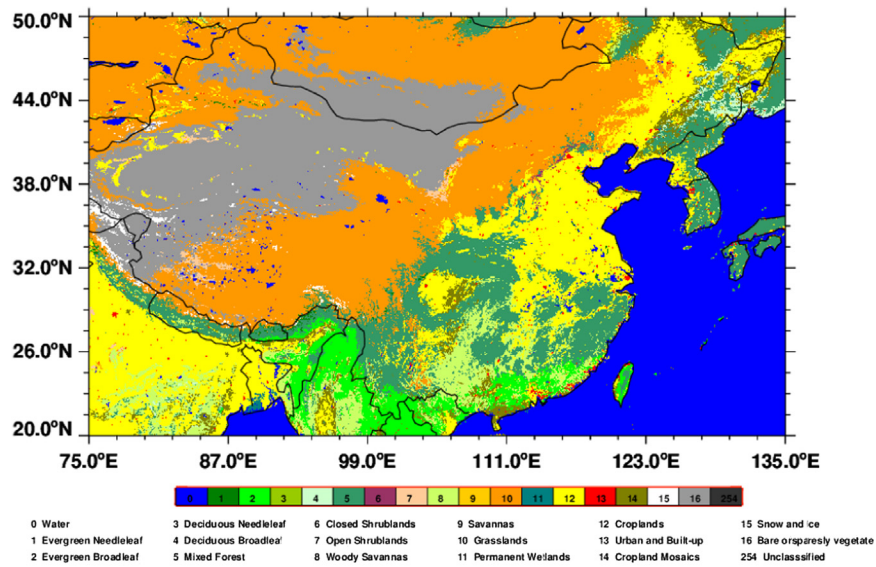


Fig. 9. China land cover distribution in 2011 from MODIS (0.05° × 0.05°).

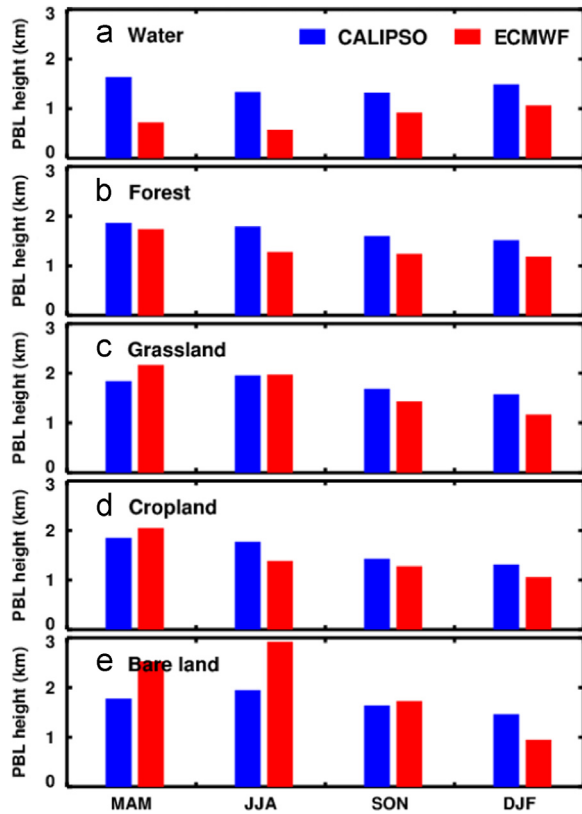


Fig. 10. Comparison of ECMWF (red) and CALIPSO (blue) seasonal PBL in the case of different land covers (water, forest, grassland, cropland, and bare land). (For interpretation of the references to color in this figure legend, the reader is referred to the web version of this article.)

Table 1
Seasonal differences in PBL height between CALIPSO and ECMWF (ECMWF PBL minus CALIPSO PBL) given different land cover conditions.

Land cover	Spring	Summer	Autumn	Winter
Water	-0.91	-0.76	-0.40	-0.42
Forest	-0.13	-0.51	-0.36	-0.34
Grassland	0.31	0.02	-0.26	-0.41
Cropland	0.20	-0.38	-0.15	-0.26
Bare land	0.75	0.97	0.09	-0.51

qualitatively reasonable, although more evaluation is needed in future work.

Acknowledgments

Supported by the National Basic Research Program of China (2012CB955301), the National Science Foundation of China (41305026), the China 111 project (No. B 13045), the Program for Changjiang Scholars and Innovative Research Team in University, and the National Science Foundation of China (41405113 and 41305027). CALIPSO data have been obtained from the Atmospheric Sciences Data Center (ASDC) at NASA Langley Research Center and PBL data have been provided by ECMWF.

References

- [1] Angevine WM, White AB, Avery SK. Boundary-layer depth and entrainment zone characterization with a boundary-layer profiler. *Boundary-Layer Meteorol* 1994;68:375–85.
- [2] Ao CO, Waliser DE, Chan SK, Li JL, Tian B, Xie F, et al. Planetary boundary layer heights from GPS radio occultation refractivity and humidity profiles. *J Geophys Res: Atmos* 2012:117.
- [3] Betts AK, Ball JH, Beljaars A, Miller MJ, Viterbo PA. The land surface–atmosphere interaction: a review based on observational and global modeling perspectives. *J Geophys Res: Atmos* (1984–2012) 1996;101:7209–25.
- [4] Chan KM, Wood R. The seasonal cycle of planetary boundary layer depth determined using COSMIC radio occultation data. *J Geophys Res: Atmos* 2013;118 (12,422–12,34).
- [5] Chen B, Huang J, Minnis P, Hu Y, Yi Y, Liu Z, et al. Detection of dust aerosol by combining CALIPSO active lidar and passive IIR measurements. *Atmos Chem Phys* 2010;10:4241–51.
- [6] Chen B, Zhang P, Zhang B, Jia R, Zhang Z, Wang T, et al. Overview of dust detection methods using passive and active satellites. *J Meteor Res* 2014;28 <http://dx.doi.org/10.1007/s13351-014-4032-4>, in press.
- [7] Chen Y, Mao X, Huang J, Zhang H, Tang Q, Pan H, et al. Vertical distribution characteristics of aerosol during a long-distance transport of heavy dust pollution. *China Environ Sci* 2009;29:449–54.
- [8] Guo P, Kuo Y-H, Sokolovskiy S, Lenschow D. Estimating atmospheric boundary layer depth using COSMIC radio occultation data. *J Atmos Sci* 2011:68.
- [9] Hansell RA, Tsay SC, Hsu NC, Ji Q, Bell SW, Holben BN, et al. An assessment of the surface longwave direct radiative effect of airborne dust in Zhangye, China, during the Asian Monsoon Years field experiment (2008). *J Geophys Res Atmos* (1984–2012) 2012:117.
- [10] Hu Y, Vaughan M, McClain C, Behrenfeld M, Maring H, Anderson D, et al. Global statistics of liquid water content and effective number concentration of water clouds over ocean derived from combined CALIPSO and MODIS measurements. *Atmos Chem Phys* 2007;7: 3353–9.
- [11] Hu Y, Vaughan M, Liu Z, Lin B, Yang P, Flittner D, et al. The depolarization-attenuated backscatter relation: CALIPSO lidar measurements vs. theory. *Opt Express* 2007;15:5327–32.
- [12] Hu Y, Winker D, Vaughan M, Lin B, Omar A, Trepte C, et al. CALIPSO/CALIP cloud phase discrimination algorithm. *J Atmos Oceanic Technol* 2009;26.
- [13] Hu Y, Rodier S, Xu K, Sun W, Huang J, Lin B, et al. Occurrence, liquid water content, and fraction of supercooled water clouds from combined CALIPSO/IIR/MODIS measurements. *J Geophys Res Atmos* (1984–2012) 2010:115.
- [14] Huang J, Minnis P, Lin B, Yi Y, Khaiyer MM, Arduini RF, et al. Advanced retrievals of multilayered cloud properties using multi-spectral measurements. *J Geophys Res: Atmos* (1984–2012) 2005: 110.
- [15] Huang J, Minnis P, Lin B, Yi Y, Fan TF, Sun-Mack S, et al. Determination of ice water path in ice-over-water cloud systems using combined MODIS and AMSR-E measurements. *Geophys Res Lett* 2006;33.
- [16] Huang J, Minnis P, Yi Y, Tang Q, Wang X, Hu Y, et al. Summer dust aerosols detected from CALIPSO over the Tibetan Plateau. *Geophys Res Lett* 2007;34.
- [17] Huang J, Zhang W, Zuo J, Bi J, Shi J, Wang X, et al. An overview of the semi-arid climate and environment research observatory over the Loess Plateau. *Adv Atmos Sci* 2008;25:906–21.
- [18] Huang J, Minnis P, Chen B, Huang Z, Liu Z, Zhao Q, et al. Long-range transport and vertical structure of Asian dust from CALIPSO and surface measurements during PACDEX. *J Geophys Res: Atmos* 2008: 113.
- [19] Huang J, Fu Q, Su J, Tang Q, Minnis P, Hu Y, et al. Taklimakan dust aerosol radiative heating derived from CALIPSO observations using the Fu-Liou radiation model with CERES constraints. *Atmos Chem Phys* 2009;9:4011–21.
- [20] Huang J, Minnis P, Yan H, Yi Y, Chen B, Zhang L, et al. Dust aerosol effect on semi-arid climate over Northwest China detected from A-Train satellite measurements. *Atmos Chem Phys* 2010;10:6863–72.
- [21] Huang J, Fu Q, Zhang W, Wang X, Zhang R, Ye H, et al. Dust and black carbon in seasonal snow across northern China. *Bull Am Meteorol Soc* 2011:92.
- [22] Jordan NS, Hoff RM, Bacmeister JT. Validation of Goddard Earth Observing System–version 5 MERRA planetary boundary layer heights using CALIPSO. *J Geophys Res: Atmos* 2010:115.
- [23] M. Kacenenbogen, M. Vaughan, J. Redemann, R. Hof, R. Rogers, R. Ferrare, P. Russell, et al., An accuracy assessment of the CALIOP/

- CALIPSO version2/version 3 daytime aerosol exti C. A. Hostetler, J.W. Hair, and B. N. Holben nction product based on a detailed multi-sensor, multi-platform case study, *Atmos Chem Phys* 11, 2011, 3981–4000.
- [24] Kai K, Nagata Y, Tsunematsu N, Matsumura T, Kim H, Matsumoto T, et al. The structure of the dust layer over the Taklimakan Desert during the dust storm in April 2002 as observed using a depolarization lidar. *J Meteorol Soc Jap Ser 2* 2008;86:1.
- [25] Klein SA, Hartmann DL. The seasonal cycle of low stratiform clouds. *J Clim* 1993;6:1587–606.
- [26] Leventidou E, Zanis P, Balis D, Giannakaki E, Pytharoulis I, Amiridis V. Factors affecting the comparisons of planetary boundary layer height retrievals from CALIPSO, ECMWF and radiosondes over Thessaloniki, Greece. *Atmos Environ* 2013;74:360–6.
- [27] Liu J, Chen B, Huang J. Discrimination and validation of clouds and dust aerosol layers over the Sahara Desert with combined CALIOP and IIR measurements. *J Meteorol Res* 2014;28:185–98.
- [28] Liu Z, Liu D, Huang J, Vaughan M, Uno I, Sugimoto N, et al. Airborne dust distributions over the Tibetan Plateau and surrounding areas derived from the first year of CALIPSO lidar observations. *Atmos Chem Phys* 2008;8:5045–60.
- [29] Margolis HA, Ryan MG. A physiological basis for biosphere–atmosphere interactions in the boreal forest: an overview. *Tree Physiol* 1997;17:491–9.
- [30] Martins J, Teixeira J, Soares PM, Miranda P, Kahn BH, Dang VT, et al. Infrared sounding of the trade-wind boundary layer: AIRS and the RICO experiment. *Geophys Res Lett* 2010;37.
- [31] McGill MJ, Vaughan MA, Trepte CR, Hart WD, Hlavka DL, Winker DM, et al. Airborne validation of spatial properties measured by the CALIPSO lidar. *J Geophys Res: Atmos* 2007;112.
- [32] McGrath-Spangler EL, Denning AS. Estimates of North American summertime planetary boundary layer depths derived from spaceborne lidar. *J Geophys Res: Atmos* 2012;117.
- [33] McGrath-Spangler EL, Denning AS. Global seasonal variations of midday planetary boundary layer depth from CALIPSO space-borne LIDAR. *J Geophys Res: Atmos* 2013;118:1226–33.
- [34] Melfi S, Spinhirne J, Chou S, Palm S. Lidar observations of vertically organized convection in the planetary boundary layer over the ocean. *J Clim Appl Meteorol* 1985;24:806–21.
- [35] Okamoto H, Nishizawa T, Takemura T, Kumagai H, Kuroiwa H, Sugimoto N, et al. Vertical cloud structure observed from shipborne radar and lidar: midlatitude case study during the MR01/K02 cruise of the research vessel Mirai. *J Geophys Res: Atmos* 2007;112.
- [36] Palm SP, Hagan D, Schwemmer G, Melfi S. Inference of marine atmospheric boundary layer moisture and temperature structure using airborne lidar and infrared radiometer data. *J Appl Meteorol* 1998;37:308–24.
- [37] Palm SP, Benedetti A, Spinhirne J. Validation of ECMWF global forecast model parameters using GLAS atmospheric channel measurements. *Geophys Res Lett* 2005;32.
- [38] Randall DA, Shao Q, Branson M. Representation of clear and cloudy boundary layers in climate models, in clear and cloudy boundary layers. *R Neth Acad Arts Sci* 1998;305–22.
- [39] Seibert P, Beyrich F, Gryning S-E, Joffre S, Rasmussen A, Tercier P. Review and intercomparison of operational methods for the determination of the mixing height. *Atmos Environ* 2000;34:1001–27.
- [40] Stull RB. An introduction to boundary layer meteorology. *Atmospheric and Oceanographic Sciences Library*; 1988.
- [41] Sugimoto N, Uno I, Nishikawa M, Shimizu A, Matsui I, Dong X, et al. Record Heavy Asian Dust in Beijing in 2002: observations and model analysis of recent events. *Geophys Res Lett* 2003;30(12):1640.
- [42] Sugimoto N, Matsui I, Shimizu A, Nishizawa T, Hara Y, Uno I. Lidar network observation of tropospheric aerosols. *SPIE Proceedings*; 2010. (p. 78600J-J-9).
- [43] Sun W, Liu Z, Videen G, Fu Q, Muinonen K, Winker DM, et al. For the depolarization of linearly polarized light by smoke particles. *J Quant Spectrosc Radiat Transfer* 2013;122:233–7.
- [44] Takamura T, Sugimoto N, Shimizu A, Uchiyama A, Yamazaki A, Aoki K, et al. Aerosol radiative characteristics at Gosan, Korea, during the atmospheric brown cloud east asian regional experiment 2005. *J Geophys Res: Atmos* 2007;112.
- [45] Teixeira J. Simulation of fog with the ECMWF prognostic cloud scheme. *Q J R Meteorol Soc* 1999;125:529–52.
- [46] Troen I, Mahrt L. A simple model of the atmospheric boundary layer; sensitivity to surface evaporation. *Boundary-Layer Meteorol* 1986;37:129–48.
- [47] Von Engel A, Teixeira J. A planetary boundary layer height climatology derived from ECMWF reanalysis data. *J Clim* 2013;26.
- [48] White A, Senff C, Banta R. A comparison of mixing depths observed by ground-based wind profilers and an airborne lidar. *J Atmos Oceanic Technol* 1999;16:584–90.
- [49] Winker D, Pelon J, McCormick M. The CALIPSO mission: spaceborne lidar for observation of aerosols and clouds. *Third International Asia-Pacific Environmental Remote Sensing Remote Sensing of the Atmosphere, Ocean, Environment, and Space: International Society for Optics and Photonics* 2003:1–11 (p.).
- [50] Winker D, Hunt W, McGill M. Initial performance assessment of CALIOP. *Geophys Res Lett* 2007;34.
- [51] Winker D, Vaughan M, Omar A, Hu Y, Powell K, Liu Z, et al. Overview of the CALIPSO mission and CALIOP data processing algorithms. *J Atmos Oceanic Technol* 2009;26.
- [52] Wood R, Bretherton C. Boundary layer depth, entrainment, and decoupling in the cloud-capped subtropical and tropical marine boundary layer. *J Clim* 2004;17.
- [53] Yan H, Huang J, Minnis P, Wang T, Bi J. Comparison of CERES surface radiation fluxes with surface observations over Loess Plateau. *Remote Sensing Environ* 2011;115:1489–500.